PAPER

Check for updates

Semiquantitative and visual detection of ferric ions in real samples using a fluorescent paper-based analytical device constructed with green emitting carbon dots†

Mengyuan He, [ID] * Yu Xiao, Yuanhang Wei and Bo Zheng

A simple and portable paper-based analytical device was developed for visual and semiquantitative detection of ferric ion in real samples using green emitting carbon dots (CDs), which were prepared *via* microwave method using sodium citrate, urea and sodium hydroxide as raw materials and then loaded on the surface of paper substrate. When Fe^{3+} exists, the green fluorescence of CDs was quenched and significant color change from green to dark blue were observed, resulting the visual detection of Fe^{3+} with a minimum distinguishable concentration of 100 μM. By analyzing the intensity changes of green channels of test paper with the help of smartphone, the semiquantitative detection was realized within the range of 100 μM to 1200 μM. The proposed paper-based analytical devices have great application prospects in on site detection of Fe^{3+} in real samples.

Introduction

As an essential element for the human body, iron plays an important role in maintaining life systems. Iron deficiency may trigger a variety of tissue changes and dysfunctions, *e.g.*, affecting the development and infection resistance of lymphoid tissues, and even worse, lead to iron deficiency anemia and decline in intelligence.[1,2] The excessive intake of iron ions will damage important human organs such as heart, liver, and lungs and cause various diseases such as tissue inflammation and cancers.[3] Besides that, Fe^{3+} widely exists in various natural environments such as animals and plants, soil, and river basin water, and in case of high content, it will be enriched in soil and water, which will affect the growth of animals and plants, and may also enter the body through the food chain to endanger human health.[4–6] Therefore, the rapid, accurate, and sensitive detection of Fe^{3+} is still necessary for environmental monitoring and human health protection.

At present, traditional methods for Fe^{3+} detection with high sensitivity and accuracy, including electrochemical analysis method, atomic absorption spectrometry (AAS), mass spectrometry (MS), liquid chromatography, and inductively coupled plasma mass spectrometry (ICP-MS) have been developed.[7–10] However, the application of these methods in metal ion detection is greatly limited because of their expensive detection equipment, complicated detection operation steps, and the need for professional personnel to test. Therefore, the development of simple and fast Fe^{3+} sensors has become the focus of attention in recent years. Among numerous new detection methods, fluorescence analysis has attracted great attention due to its advantages of simplicity and high sensitivity.[11,12]

Carbon dots (CDs) have very great potential in the detection field of fluorescent probes by virtue of high fluorescence quantum yield, stable physical and chemical properties, good water dispersibility, green synthesis process, and low costs.[13–15] In recent years, based on the quenching effect of metal ions on CDs, a serious of fluorescence sensors have been developed and can be used to detect Fe^{3+} selectively and sensitively.[16–18] However, most of the current Fe^{3+} fluorescence sensors are aimed at the detection of homogeneous solutions, needing precision instruments such as fluorescence spectrometers and the rapid on site detection of Fe^{3+} is still a great challenge.

As a new analytical method with paper as the substrate material, paper-based analytical devices (PADs) have attracted extensive attention for its advantages of easily available raw materials, low manufacturing costs, fast detection speed, and simple detection instruments.[19,20] Now a series of different optical and electrical detection methods have been developed. Among them, the fluorescence detection method, which integrates the merit of high sensitivity, has been applied in PADs in recent years.[21–23] At present, many different types of fluorescent nanoparticles, such as quantum dots,[24,25] upconversion nanoparticles,[26,27] polymer dots,[28] and noble metal nanoclusters,[29] have been used to construct paper-based fluorescent sensors

College of Chemistry and Chemical Engineering, Xinyang Normal University, Xinyang 464000, China. E-mail: myhe@xynu.edu.cn

† Electronic supplementary information (ESI) available: Partial experiments, zeta potential and FT-IR spectrum of CDs, condition optimization, selectivity of PADs and the fitting results of fluorescence lifetime. See DOI: https://doi.org/10.1039/d3ra05320b

and achieved excellent detection results. CDs have also been used as signal markers of paper-based fluorescence sensors to detect metal ions, biological small molecules, proteins and so on.[30–32] For the detection of Fe^{3+}, relatively few paper-based fluorescence sensors have been reported,[33,34] with the detection performance remaining to be further improved.

Herein, a fluorescent PADs was constructed based on green emitting CDs to realize the detection of Fe^{3+} in real water samples. CDs were prepared from sodium citrate and urea in sodium hydroxide solution through the microwave method and had bright green emission at 514 nm (Scheme 1a). The fluorescent PADs were fabricated through loading this CDs on the surface of paper substrate using a "drop-coating" method. With the introduction of Fe^{3+}, the fluorescence of CDs was quenched and the PADs showed a color change from green to dark blue. Thus the visual and semiquantitative detection of Fe^{3+} could be realized by observing the color changes with naked eye and analyzing the intensity changes of green channels with the help of smartphone respectively (Scheme 1b).

Materials and methods

Materials

Sodium citrate, urea, $FeCl_3$, sodium hydroxide (NaOH) and other inorganic salts were purchased from Sinopharm Chemical Reagent Co., Ltd. (Shanghai, China) and used as received. Dialysis membrane (MWCO = 1000) was bought from Spectrumlabs (USA). Whatman No. 1 filter paper was purchased from Whatman (UK) and used to prepare paper-based analytical devices. The ultrapure water used in this work was produced with water purification system (Milli-Q, Millipore).

Apparatus

TEM characterization of CDs was performed under a Tecnai G2 F 20 transmission electron microscope, the FT-IR spectrum was tested *via* a Nicolet 5 FT-IR spectrometer (Thermo Fisher, USA), and the zeta potential was measured using a Zetasizer Nano ZS/Mastersizer 3000E laser particle sizer (Malvern Instruments Co., Ltd., UK). In addition, the valence state of surface elements on CDs was determined using a K-ALPHA 0.5 eV X-ray photoelectron spectrometer (Thermo Scientific, USA). The fluorescence

spectra, dynamic measurements, and fluorescence lifetimes were measured through an FLS1000 (Edinburgh Instruments, UK) steady-state transient fluorescence spectrometer. The ultraviolet-visible (UV-vis) spectra of materials was acquired using a Shimadzu UV mini-1240 UV-vis spectrometer (Shimadzu Corporation, Japan). The CDs were prepared in a P70D20TL-D4 microwave oven (Galanz, China).

Preparation of green emitting CDs

The preparation of green emitting CDs was appropriately improved on the basis of the reported microwave method.[35,36] In brief, 2 g of urea and 1 g of citric acid were added in 20 mL of ultrapure water. Then 0.8 g of NaOH was introduced and stirred for 5 min. The mixed solution was heated for 5 min under the microwave condition of 700 W. After cooling to room temperature, a proper amount of ultrapure water was added for dilution, and the obtained solution was centrifuged at 8000 rpm for 3 min to remove suspended impurities. The supernatant was put into a dialysis membrane (MWCO = 1000) and purified in ultrapure water for 48 h. Finally, the concentration was adjust to 1 mg mL^{-1}.

Detection of Fe^{3+} in solution

Fe^{3+} standard solution with gradient concentration was prepared by the stepwise dilution method. 30 μL of CDs solution (1 mg mL^{-1}) and different amounts of Fe^{3+} standard solution were added into a serious of 2 mL centrifuge tubes and diluted to 600 μL with ultrapure water immediately. The fluorescence spectra were collected subsequently. To investigate the selectivity of CDs toward Fe^{3+}, Fe^{3+} and other interfering ions with the same concentration were added, and the fluorescence spectra were measured following the same steps.

Detection of Fe^{3+} on paper-based analytical devices

The circular test papers (6 mm diameter) were prepared using an office puncher. To prepare paper-based analytical devices for the detection of Fe^{3+}, 6 μL of 0.05 mg per mL CDs was added on the surface of paper and then the paper was placed at room temperature for drying. For Fe^{3+} detection, 6 μL of Fe^{3+} solution was added on the test paper and let it dry at room temperature. The fluorescence images of the test paper was taken with a smartphone under the irradiation of a 365 nm ultraviolet lamp.

Fe^{3+} detection in actual samples

The tap water sample used in this work was taken from the laboratory of our research group and filtered with filter membrane (0.22 μm) in advance to remove solid impurities. Then, Fe^{3+} was detected with the impurities-removed water as the analysis medium according to the same steps as above.

Result and discussion

Characterization of CDs

The morphology of green emitting CDs were characterized through TEM image. As shown in Fig. 1a, the prepared CDs were
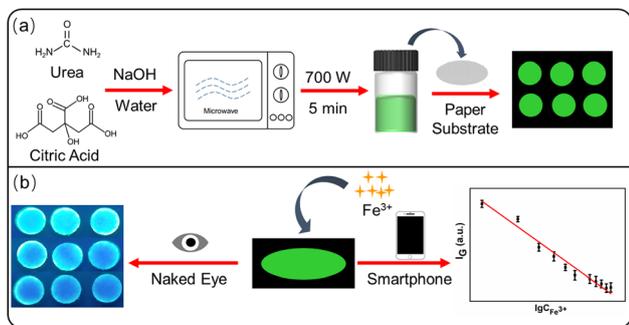
Scheme 1 Schematic illustration of the preparation of paper–based analytical devices on the basis of green emitting carbon dots (a) and the semiquantitative and visual detection of Fe^{3+} (b).
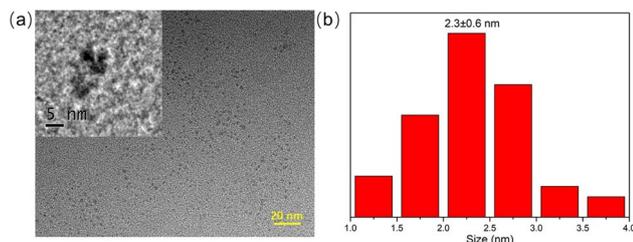
Fig. 1 (a) TEM image of CDs (inset: the HRTEM image of CDs). (b) Size distribution of CDs.

nearly spherical particles with an average particle size of 2.3 nm (Fig. 1b) and showed well dispersivity in water, which was benefit by the rich functional groups on the surface of CDs. The hydrodynamic diameter of the CDs was measured by dynamic light scattering measurements and the results demonstrated that CDs were uniformly distributed in the range of 37.8–68.0 nm (Fig. S1†). The difference compared to TEM result may be caused by the aggregation of CDs when it was dispersed in water for a long time. As depicted in Fig. S2a,† the zeta potential of CDs was −6.4 mV, indicating that the functional groups with negative charges have a slight advantage. To have a clearer understanding of surface functional groups, the FT-IR spectrum was subsequently measured. As shown in Fig. S2b,† the peak at 3393 cm^{-1} and 2940 cm^{-1} was ascribed to O–H and C–H stretching vibration, the peaks at 1567 cm^{-1} were attributed to C=O stretching vibration, the broad peak between 1465 cm^{-1} and 1392 cm^{-1} was assigned to COO^{-} symmetric stretching and C–N stretching vibration, and the peaks at 1103 cm^{-1} and 874 cm^{-1} were cause by C–O and N–H bonds, indicating the existence of various functional groups such as carboxyl and amino groups on the surface of CDs. The elemental composition and valence state of CDs were further evaluated by XPS measurements. The four main peaks at 1071.1, 531.1, 399.0, and 285.1 eV in the full-scanning XPS spectrum (Fig. 2a) were the characteristic peaks of Na 1s, O 1s, N 1s, and C 1s, with 6.92%, 27.79%, 0.84%, and 64.45% of each element,

respectively. Fig. 2b is the high-resolution XPS spectrum of C 1s, which was fitted to three peaks and assigned to C–C/C=C (284.8 eV), C–N/C–O (286.3 eV), and –COOH (288.1 eV), respectively. For O 1s (Fig. 2c), the three characteristic peaks at 531.0, 532.8, and 535.5 eV were attributed to C=O, O–H, and C–O, respectively. The two peaks at 399.2 eV and 397.7 eV in the high-resolution energy spectrum of N 1s (Fig. 2d) indicated the presence of C–N and N–H bonds. Combining with the N–H bond and C–N bond strength in FTIR spectrum, we speculated that the low nitrogen content was perhaps due to the fact that urea may be mainly used to form the core structure of CDs during the microwave synthesis process at lower power, while with a lower surface content on CDs. Overall, the above FT-IR and XPS results are consistent, indicating the existence of water-soluble functional groups such as carboxyl and amino groups, which exhibited high affinity with Fe^{3+}, ensuring the selective fluorescence response of this green emitting CDs to Fe^{3+}.

Subsequently, UV-vis spectrum and fluorescence spectra were used to characterize the optical properties of CDs. As can be observed in the UV-vis spectrum in Fig. 3a, this green emitting CDs had a characteristic absorption peak at 490 nm. The maximum excitation wavelength of CDs was located at 490 nm (Fig. 3b), which matched well with the characteristic absorption peak. Excited under this wavelength, the maximum emission wavelength of CDs was 514 nm, which was bright green (inset in Fig. 3b). Furthermore, the excitation wavelength independence test of CDs was carried out. As shown in Fig. 3c, the position of the emission peak did not change in the excitation wavelength range of 365–480 nm, indicating that CDs had independent excitation luminescence properties. The photoluminescent quantum yield (QY) of this green emitting CDs was measured and calculated to be 9.3% using of fluorescein in 0.1 M NaOH solution as a reference dye, which exhibits a quantum yield of 95% under 496 nm excitation. Meanwhile, the fluorescence stability of CDs was also measured. As depicted in Fig. 3d, the fluorescence intensity of CDs remained basically unchanged
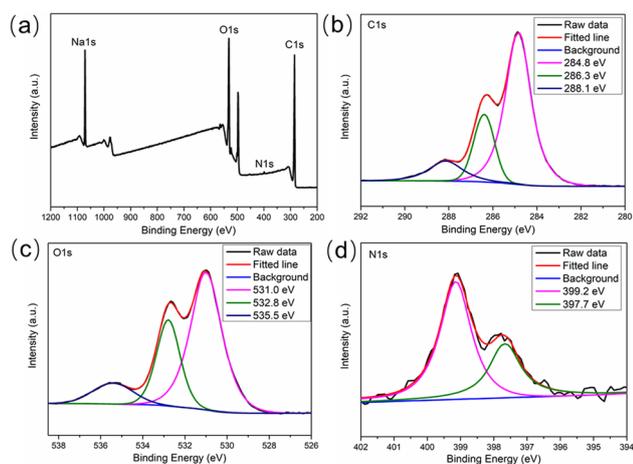

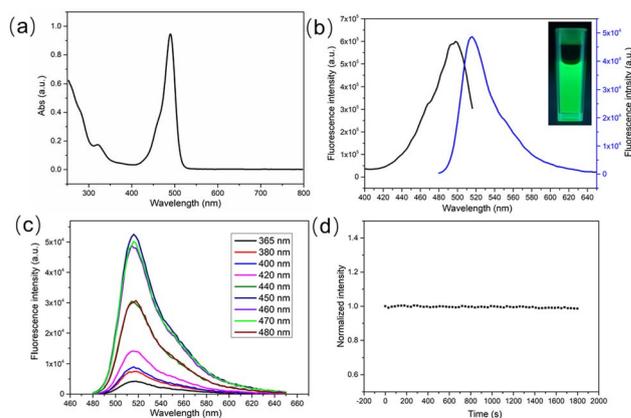**Fig. 2** (a) XPS spectra of CDs and high resolution peaks of (b) C 1s, (c) O 1s and (d) N 1s.

Fig. 3 (a) UV-vis absorption spectrum of CDs. (b) Excitation and emission spectra of CDs. (c) Emission spectra of CDs under different excitation wavelengths. (d) The fluorescence intensity of CDs at 514 nm under continuous irradiation for 30 min.

(the reduction degree was less than 3%) under the irradiation of a xenon lamp for 30 min, indicating the good fluorescence stability of the prepared CDs.

In addition, the luminescent performance of CDs is also affected by the solution environment. Therefore, the influence of pH value on the fluorescence intensity was further studied. As shown in Fig. S3a,† the pH value of the solution did not influence the position of the emission peak but would generate significant effects on the fluorescence intensity. When the pH value grew from 3 to 10, the fluorescence intensity was firstly enhanced and then declined. And the fluorescence intensity reached the maximum value under neutral conditions (Fig. S3b†). Interestingly, CDs also showed satisfying fluorescence emission behavior in pure water.

Feasibility of Fe^{3+} detection

The specific recognition of signaling molecule to target is the key to construct high-performance sensor. The abundant groups on the surface of CDs indicated that CDs were applicable to fluorescence recognition of Fe^{3+}. In order to explore the feasibility of Fe^{3+} detection, the selectivity and anti-interference of this green emitting CDs on Fe^{3+} were first studied. It could be known from Fig. 4 that when Fe^{3+} with concentration of 200 μM was added, the fluorescence of CDs was significantly quenched. To evaluate the selectivity of CDs towards Fe^{3+}, meanwhile, the influences of other over ten types of interfering metal ions, including Na^+, K^+, Ca^{2+}, Mg^{2+}, Ba^{2+}, Cu^{2+}, Pb^{2+}, Hg^{2+}, Ni^{3+}, Cr^{3+}, and Fe^{2+}, on the fluorescence signal of CDs were measured. The experimental results revealed that except Fe^{3+}, other interfering cations exerted very minor influences on the fluorescence of CDs (red histogram in Fig. 4), indicating the exclusive fluorescence response to Fe^{3+}. To explore the interference immunity of CDs, the anti-interference experiment of Fe^{3+} detection was performed under the co-existence with other metal ions. From the blue histogram in Fig. 4, it could be observed that with the presence of 200 μM interfering metal ions, the fluorescence of CDs
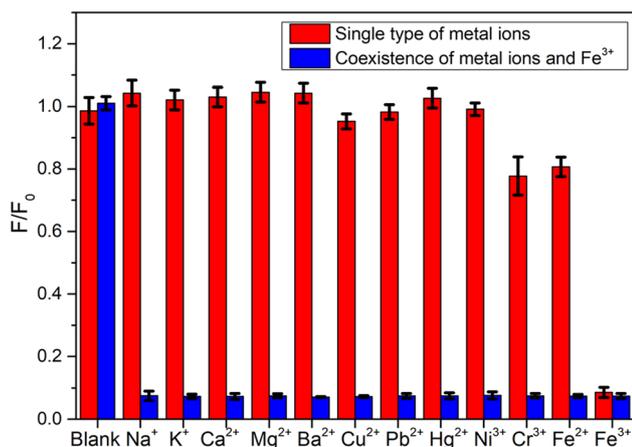

Fig. 4 The relative fluorescence intensity of CDs with the addition of single type of metal ions (Fe^{3+} and different kind of disruptors) and the coexistence of metal ion disruptors and Fe^{3+}. All of the concentrations of metal ions were 200 μM.

CDs would still be significantly quenched after the addition of Fe^{3+}. Compared with the sample only added with Fe^{3+}, the fluorescence quenching degree of CDs was basically the same under the co-existence of interfering ions, indicating that the influence of co-existing interfering ions on the detection could be ignored. The influence of ion strength on the fluorescence intensity of CDs is relatively small, and even if the concentration of disruptors reached more than twice that of Fe^{3+}, it can be clearly distinguished (Fig. S4a†). Moreover, the anion interference test were carried out and this green emitting CDs show excellent selectivity and anti-interference ability toward anions such as Cl^-, NO_3^-, and SO_4^{2-} (Fig. S4b†). The above results indicate that CDs can selectively recognize Fe^{3+} and are expected to be used in the determination of Fe^{3+} in practical samples. The excellent selectivity of this green emitting CDs towards Fe^{3+} is due to their rich functional groups on the surface, such as hydroxyl, carboxyl and amino groups, which was confirmed by FTIR spectra in Fig. S2b.† These functional groups show high affinity to Fe^{3+} and can form a complex with the Fe^{3+}, thus ensuring the selectivity of this CDs-based sensor.

Condition optimization

Since Fe^{3+} could selectively quench the fluorescence of CDs, Fe^{3+} could be detected based on the CDs fluorescence quenching method. To achieve optimal analytical performance, the experimental conditions were optimized. Considering that the fluorescence quenching degree of Fe^{3+} on CDs may vary under different pH conditions, this condition was optimized firstly. As shown in Fig. S5a,† Fe^{3+} exhibited the highest quenching degree for the fluorescence of CDs in the neutral environment pH 6 and pH 7. It is noteworthy that in pure water, Fe^{3+} also showed very excellent quenching performance for the fluorescence of CDs. For the convenience of operation, the subsequent analysis and detection process was carried out in pure water. Subsequently, the influence of the reaction time between CDs and Fe^{3+} on the fluorescence intensity was studied. As can be seen from Fig. S5b,† the fluorescence of CDs was quenched substantially as soon as Fe^{3+} was added and then kept basically unchanged with the extension of the reaction time. To obtain stable fluorescence signals, the reaction time was selected as 5 min.

Fe^{3+} detection in aqueous solutions

Under the above optimized conditions, green emitting CDs were applied to Fe^{3+} detection. As shown in Fig. 5a, with the concentration of Fe^{3+} increased from 0 μM to 400 μM, the fluorescence intensity of CDs gradually decreased. Under the low concentration of Fe^{3+} (<60 μM), the fluorescence quenching degree of CDs was relative low. When the concentration of Fe^{3+} was over 60 μM, the fluorescence quenching efficiency was significantly improved and reached the maximum under the Fe^{3+} concentration of 200 μM. As the concentration of Fe^{3+} continued to increase the fluorescence quenching efficiency was basically maintained (Fig. 5b). A good linear relationship was observed in the range of 60–200 μM (inset of Fig. 5b). The linear curve equation was $(F_0 - F)/F_0 = 0.0069[Fe^{3+}] - 0.4609$, and the correlation coefficient was $R = 0.9965$. According to $3\delta/K$ (δ is the standard deviation of
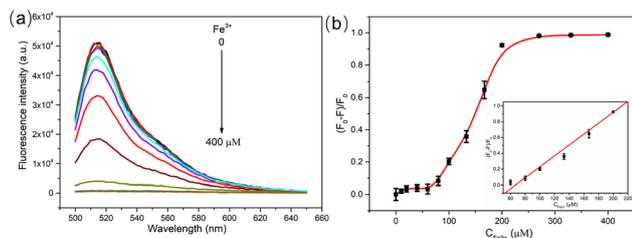
Fig. 5 (a) Fluorescence spectra of CDs (0.05 mg mL^{-1}) with the addition of different amounts of Fe^{3+} (0, 10, 20, 40, 60, 80, 100, 133, 167, 200, 270, 330, 400 μM). (b) The quenching efficiency *versus* the concentration of Fe^{3+} (inset: the linear relationship between the quenching efficiency and Fe^{3+} concentration within the range of 60–200 μM).

blank samples for 9 times and K is the slope of the linear equation), the LOD of Fe^{3+} was about 9.6 μM.

Quenching mechanism study

The fluorescence quenching modes of CDs include dynamic quenching, static quenching, fluorescence resonance energy transfer (FRET), and internal filtration effect (IFE).[37–39] Static quenching is trigged by the change of surface group structure, which leads to the decrease of fluorescence intensity, without any obvious change of fluorescence lifetime. For dynamic quenching, the fluorophores in solution collide with the quencher, which results in energy loss and the reduction of fluorescence intensity, which is most significantly characterized by the obviously shortened fluorescence lifetime of fluorophores. When there is spectral overlap between the absorption spectrum of the quencher and the excitation/emission spectrum of the fluorophore, fluorescence quenching may also be caused by IFE or FRET. The difference between them is that in the FRET process, the fluorescence lifetime of fluorophores is significantly shortened, while IFE does not affect the lifetime.

Given the above differences, the fluorescence quenching mechanism was analyzed through UV-vis spectra and fluorescence lifetime measurements. Fe^{3+} had a characteristic absorption peak in the range of 250–400 nm, but no absorption in the range of 400–800 nm (Fig. 6a), indicating no spectral overlap between CDs and Fe^{3+}, so FRET and IFE could be excluded. Given that static quenching forms non-fluorescent ground state compounds and the absorption spectrum of fluorophores will change, while the absorption spectrum does not change during
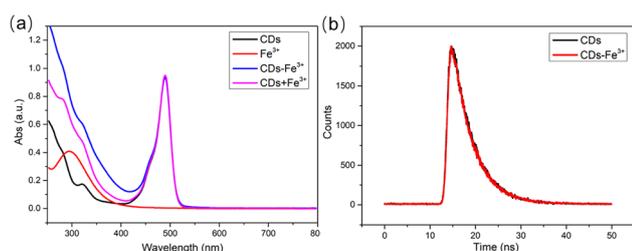
dynamic quenching, as this process only affects the excited state of the fluorescent group.[37] Therefore, the UV-vis spectra before and after the addition of Fe^{3+} were compared carefully (Fig. 6a). The results showed that after Fe^{3+} was added, the absorption spectrum of CDs–Fe^{3+} experienced shape change. The absorbance of the CDs–Fe^{3+} was not a summation of CDs and Fe^{3+} absorbance values, and the absorbance within 250–400 nm was significantly higher than the sum result, indicating that CDs and Fe^{3+} formed new non-fluorescent ground state complexes.[4,16,17] To further ascertain this speculation, zeta potential and FT-IR spectra of CDs before and after the introduction of Fe^{3+} were measured. As shown in Fig. S6a,† the zeta potential of CDs changed from −10.8 mV to 23.0 mV after been interacted with Fe^{3+}, suggesting that Fe^{3+} and N–CDs surface groups might be coordinated owing to intermolecular electrostatic interactions. Compared to the FTIR spectrum of CDs before the addition of Fe^{3+}, that after adding Fe^{3+} showed obvious changes in the intensity and slight shifts in the position of 3385 cm^{-1}, 1427 cm^{-1} and 878 cm^{-1} (Fig. S6b†), which were assigned to O–H, C=O, and N–H groups respectively. This observation might be attributed to the presence of polar functional groups, including hydroxyl, amine and carboxylic on the surface of CDs, which show strong affinity toward Fe^{3+} and form CDs–Fe^{3+} non-fluorescent complexes.[40] Subsequently, the fluorescence lifetime of CDs before and after the introduction of Fe^{3+} was measured. Fig. 6b shows the fluorescence attenuation curves before and after adding Fe^{3+} into CDs, and almost no differences were observed. The calculated average fluorescence lifetime was respectively 4.72 and 4.71 ns (Table S1†), manifesting that the fluorescence life of CDs was not affected by Fe^{3+}. The above experimental results showed that Fe^{3+} could quench the fluorescence of CDs *via* static fluorescence quenching.

Fe^{3+} detection on paper-based analytical devices

The circular filter paper was first prepared with the help of office puncher, and the paper-based analytical device for Fe^{3+}
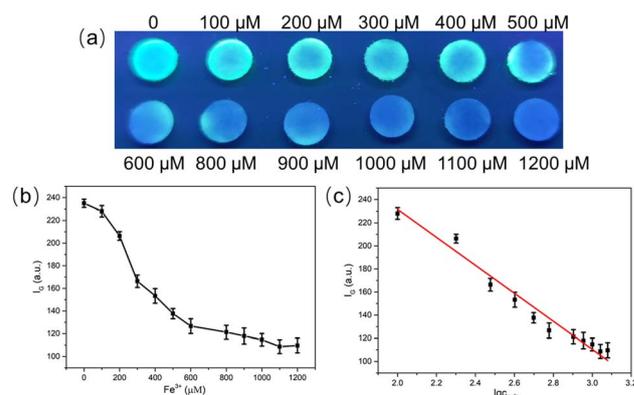

Fig. 7 (a) The images of PADs under 365 nm UV lamp with the introduction of different concentrations of Fe^{3+}. (b) The intensity of green channel of the fluorescent images *versus* the concentration of Fe^{3+}. (c) The linear relationship between the intensity of green channel and the logarithm of Fe^{3+} concentration within the range of 100–1200 μM.

Fig. 6 (a) UV-vis absorption spectra of CDs, Fe^{3+}, CDs–Fe^{3+}, and CDs + Fe^{3+}. (b) Fluorescence lifetime of CDs and CDs–Fe^{3+}.

Table 1 Comparison of different paper-based fluorescence sensors reported for Fe^{3+} detection

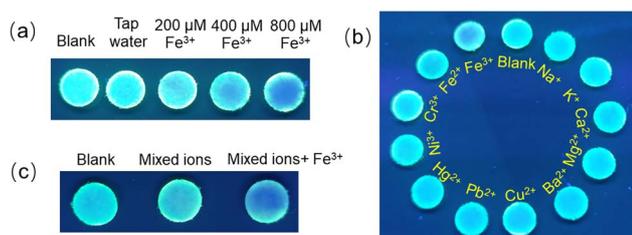| Probe	Linear range (μM)	LOD (μM)	Actual sample testing	Ref.
Nitrogen-doped carbon quantum dots	5×10^{-3} to 1×10^{-1}	9.4×10^{-4}	None	41
CdTe@SiO$_2$ QDs with rhodamine derivative	1–30	0.5	None	42
Rhodamine based probe RhBUEA	0–80	1.4	Tap water	33
Green emitting CDs	100–1200	100	Tap water	This work

Fig. 8 (a) The images of PADs under 365 nm UV lamp with the addition of different concentrations of Fe^{3+} (0, 200, 400, 800 μM) in tap water. (b) The images of PADs with the introduction of 200 μM Fe^{3+} and different kinds of interfering ions in tap water. (c) The images of PADs with the addition of mixed metal ions and their coexistence with Fe^{3+}. The concentration of Fe^{3+} and other interfering ions are all 500 μM.

detection was prepared by loading appropriate amount of CDs on the surface of paper. Under the irradiation of 365 nm ultraviolet lamp, this CDs-based PADs emitted bright green fluorescence (Fig. 7a). With the increase of Fe^{3+} concentration, the green fluorescence of CDs at 514 nm was gradually quenched, causing the color of the test paper to darken, gradually changing from bright green to dark blue. Based on this, visualization detection of Fe^{3+} can be carried out, and the naked eye distinguishable concentration reached 100 μM. For quantitative analysis, the intensity of green channel of the fluorescent image was read (expressed by I_G) via color recognition picker APP. As depicted in Fig. 7b, the I_G value was gradually reduced as the Fe^{3+} concentration increased and a good linear correlation between the I_G value and the logarithm of Fe^{3+} concentration was observed in the range of 100 μM to 1200 μM (Fig. 7c), so the quantitative analysis of Fe^{3+} could be conducted. Compared to other paper-based fluorescence sensors reported for Fe^{3+} detection, this CDs-based PADs exhibited an ultrawide linear range (more than 2 orders of magnitude), providing assurance for the detection of Fe^{3+} in actual samples (Table 1).

To investigate the selectivity of the constructed PADs to Fe^{3+}, different kinds of metal ions (500 μM) were introduced. It could be seen from Fig. S7† that the color of the PADs remained green after adding other ions, while the PADs added with Fe^{3+} turned blue obviously, indicating that this PADs had good selectivity to Fe^{3+} and could distinguish it from other interfering metal ions.

Fe^{3+} detection in actual samples

To further investigate the practicability of this strategy, the constructed PADs were used to detect Fe^{3+} in tap water. As can

be observed from Fig. 8a, when tap water was directly added into the PADs, no obvious color change could be observed. To realize Fe^{3+} detection in tap water using PADs, Fe^{3+} with different concentrations (200, 400, 800 μM) was manually introduced into tap water. When the concentration of Fe^{3+} reached 200 μM, the color change of the PADs could be distinguished by naked eyes, and its color was gradually deepened with the increase of the Fe^{3+} concentration. Furthermore, the recovery rate experiment were carried out by extracting the green channel intensity of images through smartphones. As shown in Table S2,† acceptable recovery rates ranging from 97.1% to 105.3% with RSDs less than 5% were achieved, indicating the reliability of this PADs in practical applications. In tap water samples, as depicted in Fig. 8b, this PADs could distinguish Fe^{3+} with the concentration of 200 μM from other metal ions. Considering the possible co-existence of multiple metal ions in actual water samples, a mixed ionic solution was prepared to simulate the actual water sample. It could be observed from Fig. 8c that when Fe^{3+} was contained in the mixed solution, the color of the PADs experienced significant changes, which is clearly different from the situation where Fe^{3+} does not exist. Above as, the constructed CDs-based PADs has very great feasibility and application potential in the on-site detection of Fe^{3+} in actual water samples.

Conclusion

A green emitting CDs modified paper-based analytical devices integrated with smartphone platform was developed for visual and semiquantitative detection of Fe^{3+}. CDs, which prepared through a facile and high-efficiency microwave method, had intense green light emission at 514 nm and showed specific signal response to Fe^{3+}. Dropped Fe^{3+} on fluorescent test paper would cause fluorescence quenching of CDs, resulting in the color changing from green to dark blue. The visual and semi-quantitative detection of Fe^{3+} could be realized according to the color changes of the PADs under UV light with a linear range of 100 μM to 1200 μM and a naked eye distinguishable concentration of 100 μM. The CDs-based PADs with smartphone application can render a simple, visual detection of Fe^{3+} in real water samples. The preparation method of CDs proposed in this study is simple and fast and characterized by environment-friendliness of raw materials, high luminescent intensity, fast response and selectivity to Fe^{3+}, and strong interference immunity, providing a guarantee for the excellent detection performance of PADs. Furthermore, the established fluorescent PADs, which are simple and portable, can realize Fe^{3+} detection

in water samples, showing considerable feasibility and application potential in the fast field detection of Fe^{3+}.

Author contributions

Conflicts of interest

There are no conflicts to declare.

Acknowledgements

Notes and references

1 M. Y. Hsu, E. Mina, A. Roetto and P. E. Porporato, *Cells*, 2020, **9**, 2591.

2 L. Guo, T. Tang, L. Hu, M. Yang and X. Chen, *Sens. Actuators, B*, 2017, **241**, 773–778.

3 X. Zhou, G. Zhao, X. Tan, X. Qian, T. Zhang, J. Gui, L. Yang and X. Xie, *Microchim. Acta*, 2019, **186**, 67.

4 Y. Zhou, G. Chen, C. Ma, J. Gu, T. Yang, L. Li, H. Gao, Y. Xiong, Y. Wu, C. Zhu, H. Wu, W. Yin, A. Hu, X. Qiu, W. Guan and W. Zhang, *Spectrochim. Acta, Part A*, 2023, **293**, 122414.

5 R. Atchudan, T. N. J. I. Edison, K. R. Aseer, S. Perumal, N. Karthik and Y. R. Lee, *Biosens. Bioelectron.*, 2018, **99**, 303–311.

6 S. G. Shi, Y. X. Zhang, Y. Y. Li and J. X. Chi, Au@MnO Core-shell Nanomaterials for Tumor Diagnosis and Therapy, *J. Xinyang Norm. Univ., Nat. Sci. Ed.*, 2021, **34**(4), 624–629.

7 Y. Liu, W. Duan, W. Song, J. Liu, C. Ren, J. Wu, D. Liu and H. Chen, *ACS Appl. Mater. Interfaces*, 2017, **9**, 12663–12672.

8 J. Nandre, S. Patil, V. Patil, F. Yu, L. Chen, S. Sahoo, T. Prior, C. Redshaw, P. Mahulikar and U. Patil, *Biosens. Bioelectron.*, 2014, **61**, 612–617.

9 L. S. Huang and K. C. Lin, *Spectrochim. Acta, Part B*, 2001, **56**, 123–128.

10 D. V. Biller and K. W. Bruland, *Mar. Chem.*, 2012, **130–131**, 12–20.

11 H. B. Wang, A. L. Mao, H. D. Zhang and H. Y. Bai, DNA-Au Nanoclusters-Based Novel Fluorescent Method for Sensitive Detection of Trypsin, *J. Xinyang Norm. Univ., Nat. Sci. Ed.*, 2021, **34**(1), 115–118.

12 H. B. Wang, B. B. Tao, N. N. Wu, A. L. Mao and H. D. Zhang, DNA-Au Nanoclusters Inner Filter Effect Induced Fluorescence Quenching for Sensitive Detection of 4-Nitrophenol, *J. Xinyang Norm. Univ., Nat. Sci. Ed.*, 2022, **35**(3), 464–468.

13 C. Ji, Y. Zhou, R. M. Leblanc and Z. Peng, *ACS Sens.*, 2020, **5**, 2724–2741.

14 Y. Wang, K. Jiang, J. Zhu, L. Zhang and H. Lin, *Chem. Commun.*, 2015, **51**, 12748–12751.

15 M. He, B. Zheng, N. Shang, Y. Xiao, Y. Wei and X. Hu, *Microchem. J.*, 2023, **190**, 108593.

16 M. Picard, S. Thakur, M. Misra and A. K. Mohanty, *RSC Adv.*, 2019, **9**, 8628–8637.

17 M. Amiri, A. M. H. Shabani, S. Dadfarnia, N. Shokoufi, B. Hajipour-Verdom and S. Sadjadi, *Microchim. Acta*, 2020, **187**, 562.

18 Y. Liang, L. Xu, K. Tang, Y. Guan, T. Wang, H. Wang and W. W. Yu, *Dyes Pigm.*, 2020, **178**, 108358.

19 M. He, N. Shang, Q. Zhu and J. Xu, *Anal. Chim. Acta*, 2021, **1143**, 93–100.

20 M. Wu, Q. Lai, Q. Ju, L. Li, H.-D. Yu and W. Huang, *Biosens. Bioelectron.*, 2018, **102**, 256–266.

21 F. Wang, W. Li, J. Wang, J. Ren and X. Qu, *Chem. Commun.*, 2015, **51**, 11630–11633.

22 Z. Luo, T. Lv, K. Zhu, Y. Li, L. Wang, J. J. Gooding, G. Liu and B. Liu, *Angew. Chem., Int. Ed.*, 2020, **59**, 3131–3136.

23 L. A. Pradela-Filho, W. B. Veloso, I. V. S. Arantes, J. L. M. Gongoni, D. M. de Farias, D. A. G. Araujo and T. R. L. C. Paixão, *Microchim. Acta*, 2023, **190**, 179.

24 Y. Zhou, X. Huang, C. Liu, R. Zhang, X. Gu, G. Guan, C. Jiang, L. Zhang, S. Du, B. Liu, M.-Y. Han and Z. Zhang, *Anal. Chem.*, 2016, **88**, 6105–6109.

25 X. Yuan, J. Zhang, H. Yang, Q. Yang, L. Li, M. Zhang and K. Huang, *Sens. Actuators, B*, 2022, **372**, 132686.

26 Q. Mei, H. Jing, Y. Li, W. Yisibashaer, J. Chen, B. Nan Li and Y. Zhang, *Biosens. Bioelectron.*, 2016, **75**, 427–432.

27 K. Kaur, B. K. Sahu, K. Swami, M. Chandel, A. Gupta, L.-H. Zhu, J. P. Youngblood, S. Kanagarajan and V. Shanmugam, *ACS Appl. Mater. Interfaces*, 2022, **14**, 27507–27514.

28 C. Y. Shi, N. Deng, J. J. Liang, K. N. Zhou, Q. Q. Fu and Y. Tang, *Anal. Chim. Acta*, 2015, **854**, 202–208.

29 N. Cao, J. Xu, H. Zhou, Y. Zhao, J. Xu, J. Li and S. Zhang, *Microchem. J.*, 2020, **159**, 105406.

30 Y. Kim, G. Jang and T. S. Lee, *ACS Appl. Mater. Interfaces*, 2015, **7**, 15649–15657.

31 A. Gupta, N. C. Verma, S. Khan, S. Tiwari, A. Chaudhary and C. K. Nandi, *Sens. Actuators, B*, 2016, **232**, 107–114.

32 I. Ortiz-Gomez, M. Ortega-Muñoz, A. Marín-Sánchez, I. de Orbe-Payá, F. Hernandez-Mateo, L. F. Capitan-Vallvey, F. Santoyo-Gonzalez and A. Salinas-Castillo, *Microchim. Acta*, 2020, **187**, 421.

33 X. Liu, Z. Chen, R. Gao, C. Kan and J. Xu, *J. Environ. Chem. Eng.*, 2022, **10**, 107650.

34 Y. Zhang, L. Gao, S. Ma and T. Hu, *Spectrochim. Acta, Part A*, 2022, **267**, 120525.

35 S. Qu, X. Wang, Q. Lu, X. Liu and L. Wang, *Angew. Chem., Int. Ed.*, 2012, **51**, 12215–12218.

36 J. Y. Wei, Q. Lou, J. H. Zang, Z. Y. Liu, Y. L. Ye, C. L. Shen, W. B. Zhao, L. Dong and C. X. Shan, *Adv. Opt. Mater.*, 2020, **8**, 1901938.

37 F. Zu, F. Yan, Z. Bai, J. Xu, Y. Wang, Y. Huang and X. Zhou, *Microchim. Acta*, 2017, **184**, 1899–1914.

38 X. Mu, M. Wu, B. Zhang, X. Liu, S. Xu, Y. Huang, X. Wang, D. Song, P. Ma and Y. Sun, *Talanta*, 2021, **221**, 121463.

39 M. He, N. Shang, B. Zheng and G. Yue, *RSC Adv.*, 2021, **11**, 21137–21144.

40 X. B. Cui, Y. L. Wang, J. Liu, Q. Y. Yang, B. Zhang, Y. Gao, Y. Wang and G. Y. Lu, *Sens. Actuators, B*, 2017, **242**, 1272–1280.

41 J. Korram, P. Koyande, S. Mehetre and S. N. Sawant, *ACS Omega*, 2023, **8**, 31410–31418.

42 Y. S. Kuang, X. Wang, X. K. Tian, C. Yang, Y. Li and Y. L. Nie, *J. Photochem. Photobiol., A*, 2019, **372**, 140–146.